Wigner functions for Helmholtz wave fields

Kurt Bernardo Wolf

Centro de Ciencias Físicas, Universidad Nacional Autónoma de México, Apartado Postal 48-3,
62251 Cuernavaca, México

Miguel Angel Alonso and Gregory W. Forbes

Department of Physics, Macquarie University, Sydney, NSW 2109, Australia

We investigate a general form of the Wigner function for wave fields that satisfy the Helmholtz equation in two-dimensional free space. The momentum moment of this Wigner function is shown to correspond to the flux of the wave field. For a forward-propagating wave field, the negative regions of the Wigner function are seen to be associated with small regions of backward flux in the field. We also study different projections of the Wigner function, each corresponding to a distribution in a reduced phase space that fully characterizes the wave field. One of these projections is the standard Wigner function of the field at a screen. Another projection introduced by us has the added property of being conserved along rays and is better suited to the description of nonparaxial wave fields. © 1999 Optical Society of America [S0740-3232(99)02009-8]
OCIS codes: 000.3860, 030.5630, 070.2590, 350.6980, 350.7420.

1. INTRODUCTION

The Wigner function[1] has been used most successfully in quantum mechanics and signal analysis to interpret arbitrary square-integrable functions through quasi-probability distributions on phase space. The coordinates of phase space are generally taken to be as position and its canonically conjugate momentum (or spatial frequency) under Fourier transformation. Within optics, the Wigner function of a scalar wave field at a screen was considered by Walther[2] as a possible analog of the radiance or brightness from classical radiometry. However, neither the Wigner function at a screen nor other alternatives[3,4] that have been defined possess all the properties required in the definition of the radiance, except in the case of a fully incoherent field. In particular, other than in the paraxial limit, the Wigner function at a screen of a coherent or partially coherent field is not exactly conserved along straight trajectories in free space.

Just as solutions of the Helmholtz equation are not arbitrary functions of position, their dependence on momentum (which characterizes the direction of propagation), and indeed on their initial-condition characterization on a screen, is also constrained. The Wigner function of these wave fields can be expected to exhibit the restrictions imposed by the Helmholtz equation, reducing the number of essential coordinates of its phase space. In this paper we study the Wigner function of oscillatory wave fields constrained by the two-dimensional Helmholtz equation for free space. This Wigner function is derived from the field over all space and not just over a screen (i.e., a line for two-dimensional optics), as in the conventional approach. Although in the concluding section we sketch the generalization of these ideas to three-dimensional problems, for clarity the analysis is completed here by using two-dimensional (i.e., cylindrical) waves.

In Section 2 we recall some results on Helmholtz wave fields, and in Section 3 we construct their Wigner function, checking its properties of covariance. The relation between the energy-flux density[5] of the wave field and the Wigner function is given in Section 4. In Section 5 we show that for the characterization of wave fields, it is sufficient to have a marginal distribution over a reduced phase space, and a first option is considered: the standard Wigner function mentioned above of the field at a screen. Finally, in Section 6 we propose some new alternatives and show their advantages for the study of nonparaxial wave fields.

2. HELMHOLTZ WAVE FIELDS

Solutions to the two-dimensional wave equation with a fixed, real wave number $k \in \Re^+$ are solutions $\Psi(\mathbf{q})$, $\mathbf{q} = (q_x, q_z) \in \Re^2$ of the Helmholtz equation

$$\left(\frac{\partial^2}{\partial q_x{}^2} + \frac{\partial^2}{\partial q_z{}^2} \right) \Psi(\mathbf{q}) = -k^2 \Psi(\mathbf{q}). \tag{1}$$

In particular, a plane wave that travels in the direction of the wave vector $\mathbf{k} = (k_x, k_z) = (k \sin \theta, k \cos \theta) = [k, \theta]$ (where we use square brackets to flag a polar representation), has the form

$$\Psi_{\mathbf{k}}(\mathbf{q}) \propto \exp i(k_x q_x + k_z q_z). \tag{2}$$

The restriction imposed by the Helmholtz equation on wave fields $\Psi(\mathbf{q})$ is seen clearly in the canonically conjugate momentum space $\mathbf{p} = (p_x, p_z) = (p \sin \theta, p \cos \theta) = [p, \theta] \in \Re^2$, with the Fourier transform

$$\tilde{\Psi}(\mathbf{p}) = \frac{k}{2\pi} \int_{\Re^2} \mathrm{d}^2\mathbf{q}\, \Psi(\mathbf{q}) \exp(-ik\mathbf{p} \cdot \mathbf{q}), \tag{3}$$

where $\mathrm{d}^2\mathbf{q} = \mathrm{d}q_x \mathrm{d}q_z$. With this, Eq. (1) becomes

$$(p^2 - 1)\tilde{\Psi}(\mathbf{p}) = 0 \Rightarrow \tilde{\Psi}[\mathbf{p}] = \sqrt{\frac{2\pi}{k}}\, \delta(p - 1)\psi(\theta), \quad (4)$$

so the Helmholtz equation constrains p to be unity. The function $\psi(\theta)$ on the circle $\theta \in \mathcal{S}$ is called the spectral function of the wave field. Note that, since the wave-fields of interest are nonsingular and we consider only propagation in free space, there can be no evanescent components.[6]

Free-space Helmholtz wave fields $\Psi(\mathbf{q})$ are thus determined by their spectral functions through Helmholtz wave synthesis:

$$\Psi(q_x, q_z) = \sqrt{\frac{k}{2\pi}} \int_{\mathcal{S}} \mathrm{d}\theta \psi(\theta)\exp ik(q_x \sin\theta + q_z \cos\theta). \tag{5}$$

As shown in Ref. 7, this equation can be inverted for $\psi(\theta)$ in terms of the values and normal derivatives of the wave field at the reference screen $q_z = 0$, denoted $\Psi^S(q_x) = \Psi(q_x, 0)$ and $\Psi_z^S(q_x) = \partial\Psi(q_x, q_z)/\partial q_z|_{q_z=0}$, through Helmholtz wave analysis:

$$\psi(\theta) = \frac{\sigma_z(\theta)}{2} \sqrt{\frac{k}{2\pi}} \int_{\mathfrak{R}} \mathrm{d}q_x [\Psi^S(q_x)\cos\theta$$
$$- ik^{-1}\Psi_z^S(q_x)]\exp(-ikq_x \sin\theta). \tag{6}$$

Here $\sigma_z(\theta) = \mathrm{sign}(\cos\theta)$ distinguishes between forward ($\sigma_z = +1$) and backward ($\sigma_z = -1$) wave components. When $\theta = \pm\frac{1}{2}\pi$, Eq. (6) holds in the sense of the average limit.[7]

3. WIGNER FUNCTION

The Wigner function of $\Psi(\mathbf{q})$ is defined as[1]

$$W(\Psi|\mathbf{p}, \mathbf{q}) = \left(\frac{k}{2\pi}\right)^2 \int_{\mathfrak{R}^2} \mathrm{d}^2\mathbf{r}\Psi(\mathbf{q} - \tfrac{1}{2}\mathbf{r})^*$$
$$\times \exp(-ik\mathbf{p} \cdot \mathbf{r})\Psi(\mathbf{q} + \tfrac{1}{2}\mathbf{r}) \tag{7}$$

$$= \left(\frac{k}{2\pi}\right)^2 \int_{\mathfrak{R}^2} \mathrm{d}^2\mathbf{s}\tilde{\Psi}(\mathbf{p} - \tfrac{1}{2}\mathbf{s})^*$$
$$\times \exp(+ik\mathbf{q} \cdot \mathbf{s})\tilde{\Psi}(\mathbf{p} + \tfrac{1}{2}\mathbf{s}). \tag{8}$$

Notice that the integral of the Wigner function over all its arguments yields

$$\int_{\mathfrak{R}^2} \mathrm{d}^2\mathbf{p} \int_{\mathfrak{R}^2} \mathrm{d}^2\mathbf{q} W(\Psi|\mathbf{p}, \mathbf{q}) = (\Psi, \Psi)_{\mathcal{L}^2(\mathfrak{R}^2)}$$

$$= \int_{\mathfrak{R}^2} \mathrm{d}^2\mathbf{q}\Psi(\mathbf{q})^*\Psi(\mathbf{q})$$

$$= \int_{\mathfrak{R}^2} \mathrm{d}^2\mathbf{p}\tilde{\Psi}(\mathbf{p})^*\tilde{\Psi}(\mathbf{p}), \quad (9)$$

where $(\Psi, \Psi)_{\mathcal{L}^2(\mathfrak{R}^2)}$ is the norm of $\Psi(\mathbf{q})$ in $\mathcal{L}^2(\mathfrak{R}^2)$ i.e., Lebesgue square-integrable functions over the plane. If $\Psi(\mathbf{q})$ were a quantum mechanical wave function, $\mathcal{L}^2(\mathfrak{R}^2)$ would be its appropriate Hilbert space. However, since $\Psi(\mathbf{q})$ is a Helmholtz wave field, $(\Psi, \Psi)_{\mathcal{L}^2(\mathfrak{R}^2)}$ is infinite

[see Eq. (4)], and therefore $\mathcal{L}^2(\mathfrak{R}^2)$ is not an appropriate Hilbert space for Helmholtz wave fields.

We now proceed to reduce the form of the Wigner function for Helmholtz wave fields, taking into account the results given in Section 2. From Eq. (4) we see that, as illustrated in Fig. 1, the support of the integrand of Eq. (8) consists of two points when $p < 1$ and none when $p > 1$. In the second case the Wigner function is therefore zero. In the first case there will be contributions from the points where the argument vectors $\mathbf{p} - \frac{1}{2}\mathbf{s}$ and $\mathbf{p} + \frac{1}{2}\mathbf{s}$ simultaneously intersect the unit circle. On the integration plane $\mathbf{s}$ this occurs at the angles $\theta \mp \frac{1}{2}\varpi$, where θ is the angular coordinate of $\mathbf{p} = [p, \theta]$, and $\cos\frac{1}{2}\varpi = p$. This shows qualitatively that the Wigner function of Helmholtz wave fields can be found in closed form in terms of their spectral functions on the circle. Further, it is singular at both $p = 0$ and $p = 1$.

By using Eq. (5), we introduce the spectral functions on the circle, exchange integrals, and use the Dirac δs that appear, to find

$$W(\Psi|\mathbf{p}, \mathbf{q}) = \frac{k}{2\pi} \int_{\mathcal{S}} \mathrm{d}\theta \int_{\mathcal{S}} \mathrm{d}\theta' \psi(\theta)^*\psi(\theta')$$
$$\times \delta[p_x - \tfrac{1}{2}(\sin\theta + \sin\theta')]$$
$$\times \delta[p_z - \tfrac{1}{2}(\cos\theta + \cos\theta')]$$
$$\times \exp\{-ik[q_x(\sin\theta - \sin\theta')$$
$$+ q_z(\cos\theta - \cos\theta')]\}$$
$$= \frac{k}{2\pi} \int_{\mathcal{S}} \mathrm{d}\alpha \int_{-\pi}^{\pi} \mathrm{d}\beta \psi(\alpha - \tfrac{1}{2}\beta)^*\psi(\alpha + \tfrac{1}{2}\beta)$$
$$\times \delta(p_x - \cos\tfrac{1}{2}\beta \sin\alpha)$$
$$\times \delta(p_z - \cos\tfrac{1}{2}\beta \cos\alpha)$$
$$\times \exp[2ik(q_x\cos\alpha - q_z\sin\alpha)\sin\tfrac{1}{2}\beta].$$
$$(10)$$

The last expression suggests a convenient change of variables to the vector $\mathbf{t} = [\cos\frac{1}{2}\beta, \alpha]$, so the product of deltas simply becomes $\delta(\mathbf{p} - \mathbf{t})$, and the measure is $\mathrm{d}\beta\mathrm{d}\alpha = 2\mathrm{d}^2\mathbf{t}/t\sqrt{1 - t^2}$ for $\mathbf{t}$ inside the unit circle. Thus we write the Wigner function expressed in polar coordinates $\mathbf{p} = [p, \theta]$ of the momentum plane, for $0 < p < 1$,
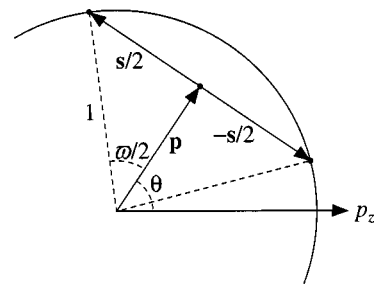
Fig. 1. Support of the integrand of Eq. (8) consists of two points, where the momentum arguments of the two functions, the vectors $\mathbf{p} - (1/2)\mathbf{s}$ and $\mathbf{p} + (1/2)\mathbf{s}$, meet the unit circle.

$$W(\Psi|\mathbf{p}, \mathbf{q}) = \frac{k}{\pi p\sqrt{1 - p^2}}\{\psi(\theta - \tfrac{1}{2}\varpi)^*\psi(\theta + \tfrac{1}{2}\varpi)$$

$$\times \exp[2ik\sqrt{1 - p^2}(q_x\cos\theta - q_z\sin\theta)]$$

$$+ \psi(\theta + \tfrac{1}{2}\varpi)^*\psi(\theta - \tfrac{1}{2}\varpi)$$

$$\times \exp[-2ik\sqrt{1 - p^2}$$

$$\times (q_x\cos\theta - q_z\sin\theta)]\}, \tag{11}$$

where

$$\varpi = 2\arccos p \in (0, \pi). \tag{12}$$

Recall that $W(\Psi|\mathbf{p}, \mathbf{q})$ is zero for $p > 1$. Equation (11) gives the closed form spoken of above.

As expected, the real-valued expression given in Eq. (11) exhibits singularities at $p = 0$ and $p = 1$. Also, the combination $q_x\cos\theta - q_z\sin\theta$ that appears in the exponents is the cross product between the position vector $\mathbf{q}$ and a unit vector in the direction of the momentum vector $\mathbf{p}$. In fact, since W depends on q_x and q_z only through this combination, it satisfies

$$W(\Psi|\mathbf{p}, q_x, q_z) = W(\Psi|\mathbf{p}, q_x - q_z\tan\theta, 0). \tag{13}$$

That is, for each value of $\mathbf{p}$, $W(\Psi|\mathbf{p}, \mathbf{q})$ is constant for all values of $\mathbf{q}$ that fall along any line parallel to $\mathbf{p}$. Therefore a displacement along the z axis corresponds to a nonlinear shear of the remaining three-dimensional space. Finally, we note that under Euclidean transformations of the plane, that is, under translations

$$\mathcal{T}_\mathbf{u}: \Psi(\mathbf{q}) = \Psi(\mathbf{q} + \mathbf{u}),$$

$$\mathcal{T}_\mathbf{u}: \psi(\theta) = \exp[ik(u_x\sin\theta + u_z\cos\theta)]\psi(\theta), \tag{14}$$

and rotations represented by 2×2 matrices $\mathbf{R}(\beta)$,

$$\mathcal{R}_\beta: \Psi(\mathbf{q}) = \Psi[\mathbf{R}(\beta)\mathbf{q}], \qquad \mathcal{R}_\beta: \psi(\theta) = \psi(\theta + \beta), \tag{15}$$

the Wigner function is *covariant*, i.e.,

$$W(\mathcal{T}_\mathbf{u}\Psi|\mathbf{p}, \mathbf{q}) = W(\Psi|\mathbf{p}, \mathbf{q} + \mathbf{u}), \tag{16}$$

$$W(\mathcal{R}_\beta\Psi|\mathbf{p}, \mathbf{q}) = W(\Psi|\mathbf{R}(\beta)\mathbf{p}, \mathbf{R}(\beta)\mathbf{q}). \tag{17}$$

Notice that, as opposed to quantum mechanical wave functions, Helmholtz wave fields cannot be translated in momentum because their support circle must remain in place. [That is, the product of a Helmholtz wave field and a phase factor $\exp(ik\mathbf{s} \cdot \mathbf{q})$ is not a Helmholtz wave field.]

4. PROJECTIONS AND MOMENTS OF THE WIGNER FUNCTION: INTENSITY AND FLUX OF WAVE FIELDS

In this section we examine quantities derived from the Wigner function that have a more direct physical meaning. By integrating the Wigner function [Eq. (7)] over momentum space $\mathbf{p} \in \mathfrak{R}^2$, after an exchange of integrals, one recovers the squared amplitude of the field, loosely called the intensity:

$$I(\Psi|\mathbf{q}) = \int_{\mathfrak{R}^2} d^2\mathbf{p}\, W(\Psi|\mathbf{p}, \mathbf{q}) = |\Psi(\mathbf{q})|^2. \tag{18}$$

Equivalently, one can show from Eq. (8) that the integral of the Wigner function over position space $\mathbf{q} \in \mathfrak{R}^2$ gives the squared amplitude of the momentum representation of the field, defined in Eq. (3). However, as can be seen from Eq. (4), this quantity is not well defined: It is zero over all $\mathbf{p}$ except for $p = 1$, where it is infinite. The first moment of the position vector of the Wigner function, given by the integral over all $\mathbf{q} \in \mathfrak{R}^2$ of $\mathbf{q}W$ is also ill-defined. On the other hand, the first moment of the momentum vector of the Wigner function yields the local flux[5] of the wave field:

$$\mathbf{J}(\Psi|\mathbf{q}) = \int_{\mathfrak{R}^2} d^2\mathbf{p}\,\mathbf{p}\, W(\Psi|\mathbf{p}, \mathbf{q})$$

$$= \frac{i}{k}\left(\frac{k}{2\pi}\right)^2 \int_{\mathfrak{R}^4} d^2\mathbf{p}\, d^2\mathbf{r}\, \Psi(\mathbf{q} - \tfrac{1}{2}\mathbf{r})^*$$

$$\times [\nabla_\mathbf{r}\exp(-ik\mathbf{p} \cdot \mathbf{r})]\Psi(\mathbf{q} + \tfrac{1}{2}\mathbf{r})$$

$$= \frac{i}{2k}\left(\frac{k}{2\pi}\right)^2 \int_{\mathfrak{R}^4} d^2\mathbf{p}\, d^2\mathbf{r}[-\Psi(\mathbf{q} + \tfrac{1}{2}\mathbf{r})$$

$$\times \nabla_\mathbf{q}\Psi(\mathbf{q} - \tfrac{1}{2}\mathbf{r})^*$$

$$+ \Psi(\mathbf{q} - \tfrac{1}{2}\mathbf{r})^*\nabla_\mathbf{q}\Psi(\mathbf{q} + \tfrac{1}{2}\mathbf{r})]\exp(-ik\mathbf{p} \cdot \mathbf{r})$$

$$= \frac{1}{2ik}[\Psi(\mathbf{q})\nabla_\mathbf{q}\Psi(\mathbf{q})^* - \Psi(\mathbf{q})^*\nabla_\mathbf{q}\Psi(\mathbf{q})]$$

$$= \frac{1}{k}\mathrm{Im}[\Psi(\mathbf{q})\nabla_\mathbf{q}\Psi(\mathbf{q})^*]. \tag{19}$$

This quantity explicitly satisfies $\nabla \cdot \mathbf{J} = 0$, and Eq. (19) clearly reinforces the intuitive connection to classical radiometry. Notice from Eq. (19) that for stationary Helmholtz fields (which have constant phase), the flux is zero.

In Fig. 2 we show the flux-vector field for a forward-rectangle beam given by the spectral function $\psi(\theta) = \rho(\theta; \pi/2)$, where

$$\rho(\theta; \omega) = (2\omega)^{-1}\mathrm{Rect}_\omega(\theta) = \begin{cases} 1/2\omega & |\theta| < \omega, \\ 0 & \text{otherwise} \end{cases}. \tag{20}$$

As expected, the flux-vector field is maximal in the forward z direction at the center of the beam, spreading out as it advances in the z axis. At the waist of the beam, on the $q_z = 0$ line, notice the appearance of vortices[8] and saddle points of the flux vectors. Although the magnitude of the flux itself is then small, there are intervals along this axis where it flows backward, despite the fact that the beam is composed solely of forward-propagating plane waves. One can study the behavior of the flux at the x axis analytically by computing the field and its derivatives:
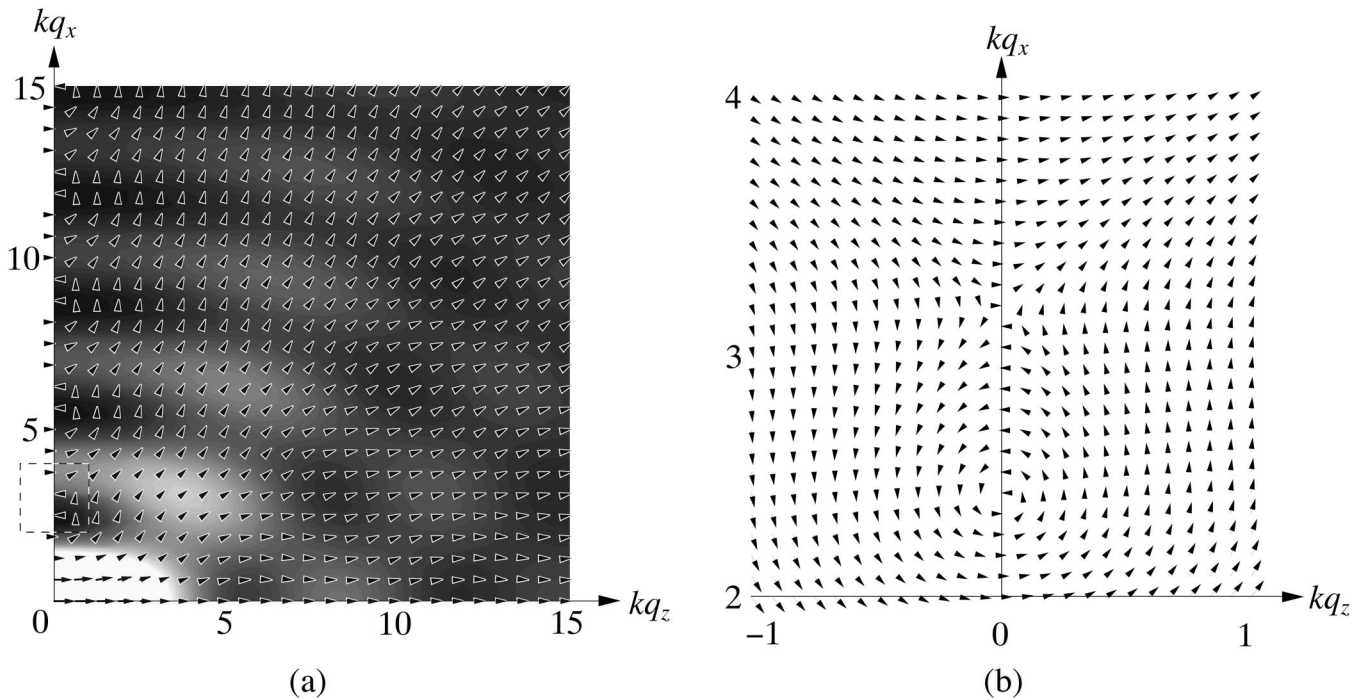
Fig. 2. (a) Intensity and flux-vector field of a forward rectangle beam with spectral function $\psi(\theta) = \mathrm{Rect}_{\pi/2}(\theta)$. Note that beyond the field waist there are flux vortices, and saddle points along the x axis. The flux-vector field for the region inside the dotted box is shown in detail in (b).

$$\Psi(q_x, 0) = \sqrt{\frac{k}{2\pi}} \int_{-\pi/2}^{\pi/2} \mathrm{d}\theta \, \exp(ikq_x \sin\theta)$$

$$= \sqrt{\frac{k}{2\pi}} J_0(kq_x), \tag{21}$$

$$\Psi_{q_x}(q_x, 0) = ik \sqrt{\frac{k}{2\pi}} \int_{-\pi/2}^{\pi/2} \mathrm{d}\theta \, \sin\theta \, \exp(ikq_x \sin\theta)$$

$$= -k\pi \sqrt{\frac{k}{2\pi}} J_1(kq_x), \tag{22}$$

$$\Psi_{q_z}(q_x, 0) = ik \sqrt{\frac{k}{2\pi}} \int_{-\pi/2}^{\pi/2} \mathrm{d}\theta \, \cos\theta \, \exp(ikq_x \sin\theta)$$

$$= 2ik \sqrt{\frac{k}{2\pi}} \frac{\sin kq_x}{q_x}, \tag{23}$$

where J_0 and J_1 are Bessel functions. Because the q_x derivative is real, the x component of the flux is zero at the waist line. We thus find the flux to be purely along the z axis, with values

$$J_z(\Psi|q_x, 0) = \frac{k}{\pi} J_0(kq_x) \frac{\sin kq_x}{q_x}. \tag{24}$$

The flux will be backward where the two functions on the right-hand side of Eq. (24) have opposite signs, i.e., between $kq_x = 2.4048...$ and $3.1416...$, etc., as can be seen in Fig. 2.

It turns out that these regions of backward flux are related to the negative regions of the Wigner function: It
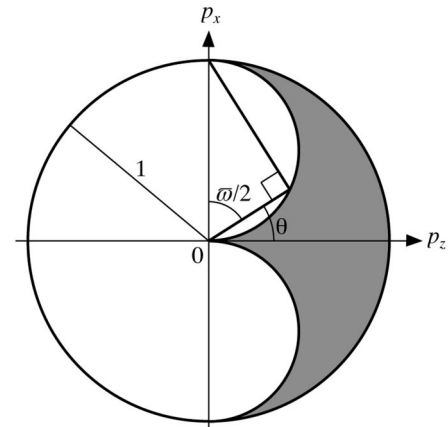
Fig. 3. Gray area represents support in momentum for the Wigner function of a forward-propagating field.

was mentioned above that the Wigner function is different from zero only for $|\mathbf{p}| \leq 1$. For a forward-propagating wave field, the support in momentum of the Wigner function is even more restricted: We can see that in this case, the Wigner function defined in Eqs. (11) and (12) vanishes outside the region shown in Fig. 3 and defined by $|\theta| \leq \pi/2 - \arccos p$, $0 \leq p \leq 1$. Since $p_z \geq 0$ at all points in this region, the moment given in Eq. (19) can have a negative z component only if W takes predominantly negative values. This is verified in Fig. 4, where, for the wave field considered above, we show $p\sqrt{1 - p^2} W(\Psi|\mathbf{p}, \mathbf{q})$ evaluated at the center of the beam $k\mathbf{q} = (0, 0)$ and at $k\mathbf{q} = (2.7, 0)$, which corresponds to a point of backward flux in Fig. 2 and where we see predominantly negative values.

5. SCREEN MARGINAL

In Section 3 the Wigner function of two-dimensional Helmholtz wave fields was found as a function of four variables, $\mathbf{p} = (p_x, p_z)$ and $\mathbf{q} = (q_x, q_z)$, with the restriction that it be zero for $|\mathbf{p}| > 1$. Four-dimensional distributions are of course inconvenient for visualizing the properties of two-dimensional wave fields. To reduce the number of dimensions, it is convenient to find subspaces and/or projections of W (referred to here as marginals) that give a useful description of the wave field. One such marginal is the intensity given in Eq. (18), which depends on position variables only. However, other options are better suited for certain applications. A standard alternative, referred to here as the screen marginal, follows from integrating W over $p_z \in \Re$. From Eq. (7),

$$K(\Psi|p_x, q_x; q_z) = \int_{\Re} dp_z W(\Psi|\mathbf{p}, \mathbf{q})$$

$$= \frac{k}{2\pi} \int_{\Re} dr_x \Psi(q_x - \tfrac{1}{2}r_x, q_z)^*$$

$$\times \exp(-ikp_x r_x)\Psi(q_x + \tfrac{1}{2}r_x, q_z).$$

(25)

At a screen of fixed q_z, K is a function of the conjugate variables p_x and q_x, and it has the same form as W itself. The screen marginal is the form of the Wigner function that has been widely used in wave optics.[9] Wolf and Rivera[10] considered the holographic information contained in the interference component of the screen marginal of two superimposed beams. Bastiaans[11] used the screen marginal as a connection between ray and wave optics in the paraxial domain. As mentioned in Section

1, K has been proposed as a possible wave analog of the radiance from classical radiometry. The radiance has the property of being constant at all the points that form a straight line in a specified direction. Remember from Eq. (13) that W satisfies a similar property. However, for coherent fields (and even for partially coherent fields), the screen marginal presents this property only in the paraxial limit. That is, it is not constant for all sets of values of $p_x = \sin\theta$, q_x, and q_z that correspond to the same straight line in $\mathbf{q}$ space, referred to here as a ray. [Notice that these quantities identify a ray uniquely only under the assumption that the field propagates exclusively in the forward (or backward) z direction.] Only for wave fields propagating paraxially in the positive z direction [i.e., when $\psi(\theta)$ takes significant values only for $|\theta| \ll \pi/2$], can it be shown from Eq. (25) that the screen marginal satisfies

$$K(\Psi|p_x, q_x; q_z) \approx K(\Psi|p_x, q_x - p_x q_z, 0). \quad (26)$$

Approximation (26) implies that the only effect of a displacement in the z axis is a linear shear in the (q_x, p_x) plane, so K is "conserved" along paraxial rays. Beyond the paraxial approximation, however, this property does not hold, and the effect of a displacement in z is not just a deformation of K in the (q_x, p_x) plane but a more complicated redistribution in which ripples are typically introduced in the vicinity of any concavity of the domain in which K takes nonnegligible values.

To visualize these effects, let us consider the rectangle beam defined in Eq. (20). Notice that the limit $\omega \to 0^+$ represents a Dirac δ in angle and a plane wave in optical $\mathbf{q}$ space, while the widest case $\omega \to \pi^-$ corresponds to a monopole field $\sim J_0(k|\mathbf{q}|)$ that has maximal localization in $\mathbf{q}$ space. In Figs. 5 and 6 we present the cases $\omega = \pi/16$ and $\omega = \pi/4$, respectively, and show (a) the spec-
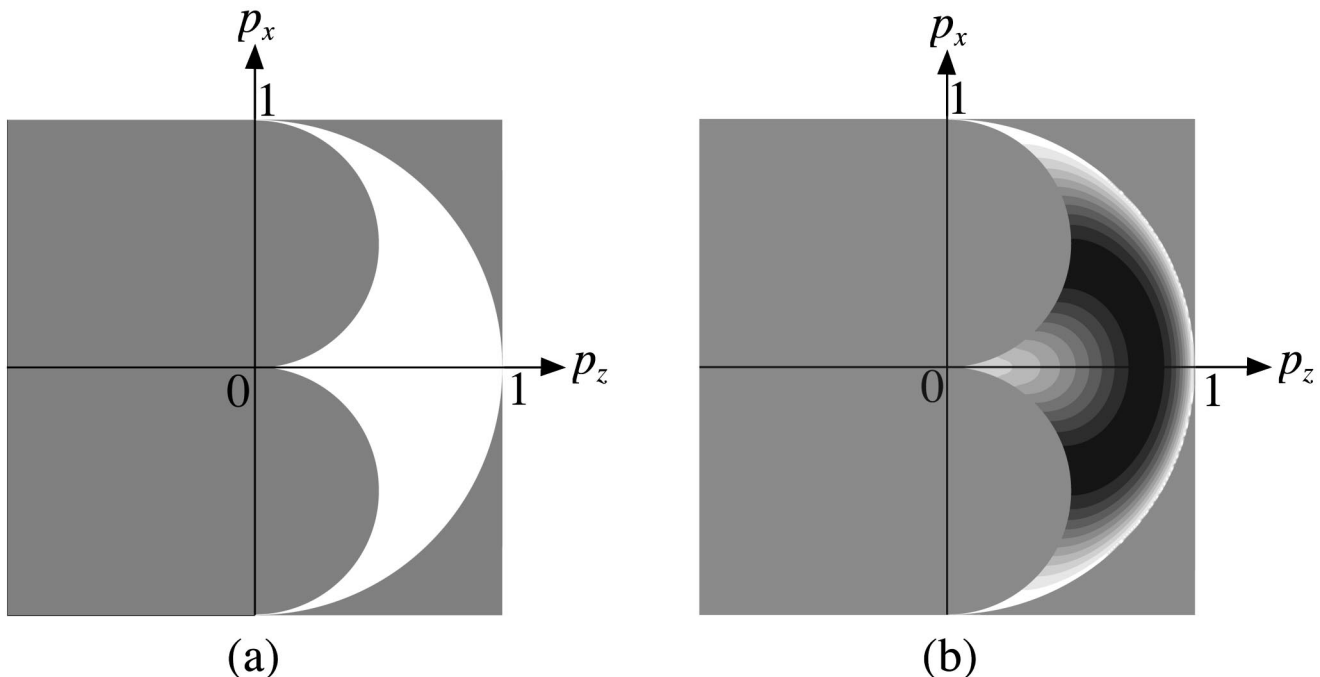
Fig. 4. $p\sqrt{1 - p^2}\, W(\Psi|\mathbf{p}, \mathbf{q})$ for a forward-rectangle beam, evaluated at (a) $k\mathbf{q} = (0, 0)$ and (b) $k\mathbf{q} = (2.7, 0)$. The shade of gray in the background of both figures corresponds to zero, and lighter (darker) shades of gray correspond to higher (lower) values.
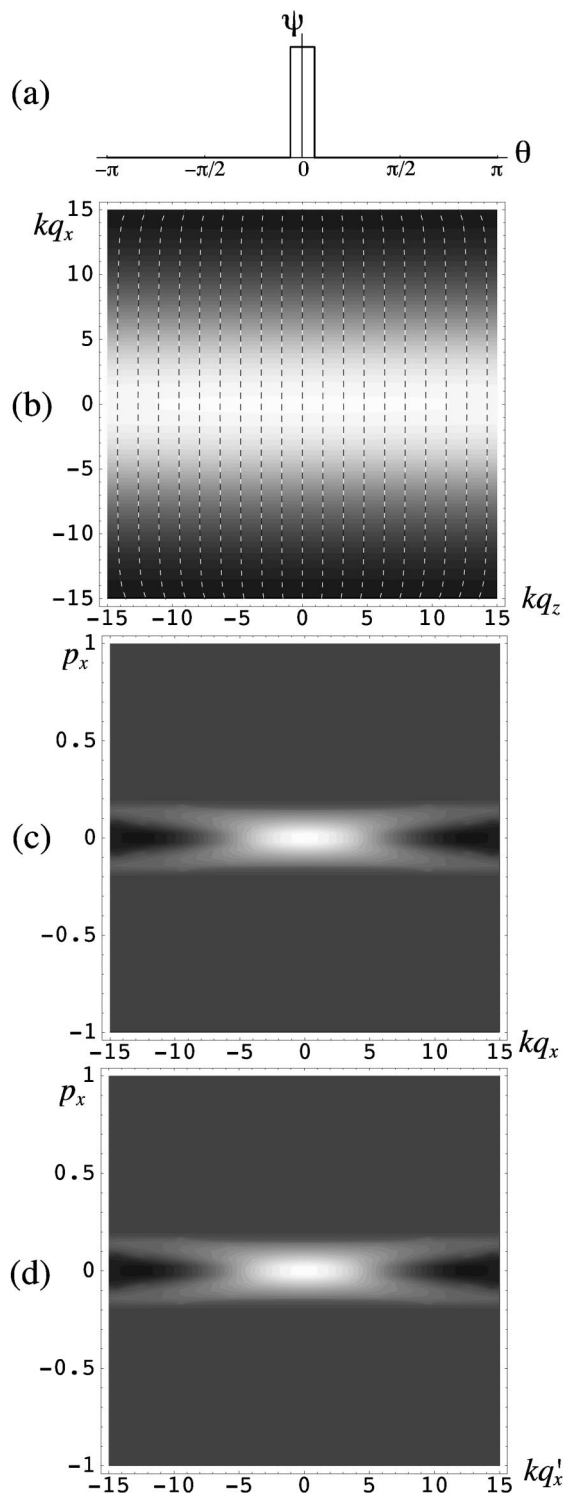
Fig. 5.   For a rectangle beam of width $w = \pi/16$, as defined by Eq. (20):   (a) spectral function on the circle, (b) intensity and wave fronts of the wave field on the **q** plane, (c) screen marginal at $q_z = 0$, and (d) screen marginal at $kq_z = 50$, where $q'_x = q_x + p_x q_z/\sqrt{1 - p_x^2}$.

Fig. 6.   For a rectangle beam of width $w = \pi/4$, as defined by Eq. (20):   (a) spectral function on the circle, (b) intensity and wave fronts of the wave field on the **q** plane, (c) screen marginal at $q_z = 0$, and (d) screen marginal at $kq_z = 50$, where $q'_x = q_x + p_x q_z/\sqrt{1 - p_x^2}$.

tral function $\psi(\theta) = \rho(\theta; \omega)$ in Eq. (20), (b) the intensity $I(\Psi|\mathbf{q})$ in Eq. (18), and (c) the screen marginal $K(\Psi|p_x, q_x; 0)$ in Eq. (25).   To show that the screen marginal is conserved along rays only in the paraxial limit, we also show (d) $K(\Psi|p_x, q_x - p_x q_z/\sqrt{1 - p_x^2}; q_z)$ for

$kq_z = 50$.   Notice that the discrepancies between (c) and (d) are much more noticeable in Fig. 6 than in Fig. 5.

The screen marginal has other, more significant problems: It presents singularities for some nonparaxial fields.   From Eqs. (10) and (25), we can write the screen

marginal at $q_z = 0$ in terms of the spectral functions:

$$K(\Psi|p_x, q_x; 0)$$

$$= \frac{k}{2\pi} \int_{\mathcal{S}} \mathrm{d}\alpha \int_{-\pi}^{\pi} \mathrm{d}\varpi \, \psi(\alpha - \tfrac{1}{2}\varpi)^*$$

$$\times \psi(\alpha + \tfrac{1}{2}\varpi)\delta(p_x - \cos\tfrac{1}{2}\varpi \sin\alpha)$$

$$\times \exp[2ik(q_x \cos\alpha - q_z \sin\alpha)\sin\tfrac{1}{2}\varpi], \quad (27)$$

which, evaluated at $p_x = 0$, gives

$$K(\Psi|0, q_x; 0) = \frac{k}{2\pi} \int_{-\pi}^{\pi} \frac{\mathrm{d}\varpi}{\cos\tfrac{1}{2}\varpi}[\psi(-\tfrac{1}{2}\varpi)^*\psi(\tfrac{1}{2}\varpi)$$

$$\times \exp(2ikq_x \sin\tfrac{1}{2}\varpi)$$

$$+ \psi(\pi - \tfrac{1}{2}\varpi)^*\psi(\pi + \tfrac{1}{2}\varpi)$$

$$\times \exp(-2ikq_x \sin\tfrac{1}{2}\varpi)]. \quad (28)$$

When $\psi(\theta)$ is nonzero near $|\theta| = \pi/2$, the integral in Eq. (28) diverges. To understand this problem, consider the integral of the screen marginal over its conjugate arguments $p_x \in \mathfrak{R}$ and $q_x \in \mathfrak{R}$. From Eqs. (25) and (27) respectively, these integrals lead to

$$\int_{\mathfrak{R}} \mathrm{d}p_x \int_{\mathfrak{R}} \mathrm{d}q_x K(\Psi|p_x, q_x; q_z)$$

$$= \int_{\mathfrak{R}} \mathrm{d}q_x \Psi(q_x, q_z)^*\Psi(q_x, q_z) \quad (29)$$

$$= \int_{\mathcal{S}} \mathrm{d}\theta \frac{|\psi(\theta)|^2}{|\cos\theta|}. \quad (30)$$

Equation (29) tells us that for fixed q_z, the integral of the screen marginal over p_x and q_x corresponds to the norm for the Hilbert space $\mathcal{L}^2(\mathfrak{R})$ of wave fields at that screen. However, from Eq. (30) we can see that this norm is not necessarily finite: We need $|\psi(\theta)| \to 0$ as $|\theta| \to \pi/2$. Furthermore, for this Hilbert space, the norm of a field changes after a rotation. For example, the norm of a rectangle beam $\psi(\theta) = \rho(\theta + \beta; \omega)$, for $\omega < \pi/2$, is minimal at $\beta = 0$ and diverges for $\pi/2 - \omega \le |\beta| \le \pi/2 - \omega$. A rectangle beam with $\omega \ge \pi/2$ (like the one considered in Section 4), always has an infinite norm in the Hilbert space $\mathcal{L}^2(\mathfrak{R})$, and therefore its screen marginal is singular.

6. ANGLE-POSITION AND ANGLE-IMPACT MARGINALS

We now define a new marginal distribution that is fully covariant and for which q_z is truly redundant because of Eq. (13). Notice that K has neither of these properties because it was constructed by the projection of W over one component of momentum. Instead, we now integrate W over p. Integration of Eq. (10) with the natural radial measure p yields the angle-position marginal

$$L(\Psi|\theta, q_x; q_z) = \int_0^1 p \mathrm{d}p \, W(\Psi|\mathbf{p}, \mathbf{q})$$

$$= \frac{k}{2\pi} \int_{-\pi}^{\pi} \mathrm{d}\alpha \, \psi(\theta - \tfrac{1}{2}\alpha)^*\psi(\theta + \tfrac{1}{2}\alpha)$$

$$\times \exp[2ik(q_x \cos\theta - q_z \sin\theta)\sin\tfrac{1}{2}\alpha]. \quad (31)$$

This function carries the essential characterization of Helmholtz wave fields. It inherits the reality condition from W (as did K), as well as covariance under Euclidean transformations of the plane (14)–(17). Notice from Eq. (31) that L satisfies a property that follows from Eq. (13):

$$L(\Psi|\theta, q_x; q_z) = L(\Psi|\theta, q_x - q_z \tan\theta; 0). \quad (32)$$

That is, L is exactly conserved along rays (even for coherent wave fields composed of plane waves that propagate in all directions), and the evolution of a wave field along the z axis corresponds precisely to a nonlinear shear of the original distribution in the (q_x, θ) plane—which may be thought of as a cylinder. In the paraxial case, one can show that

$$K(\Psi|\sin\theta, q_x; q_z) \approx L(\Psi|\theta, q_x; q_z). \quad (33)$$

Notice that the quantity $\mathbf{q} \times \mathbf{p} = q_x \cos\theta - q_z \sin\theta$ is conserved along a ray, and in fact it corresponds to the ray's angular momentum l (since the magnitude of the linear momentum of a ray is equal to the refractive index, which is unity here). Geometrically, the magnitude of l corresponds to the impact parameter, which is the closest approach of the ray to the origin, and its sign indicates the sense of rotation. Since the conjugate variables θ and l uniquely identify a ray, it is natural to define the angle-impact marginal as

$$M(\Psi|\theta, l) = \frac{k}{2\pi} \int_{-\pi}^{\pi} \mathrm{d}\alpha \, \psi(\theta - \tfrac{1}{2}\alpha)^*\psi(\theta + \tfrac{1}{2}\alpha)$$

$$\times \exp(2ikl \sin\tfrac{1}{2}\alpha) \quad (34)$$

such that

$$L(\Psi|\theta, q_x; q_z) = M(\Psi|\theta, q_x \cos\theta - q_z \sin\theta).$$

The phase-space picture afforded by the angle-position and angle-impact marginals is also complete, because—up to an overall phase—we can recover the spectral functions of Helmholtz wave fields through integration of Eq. (31) over its position variable $q_x \in \mathfrak{R}$, with a phase factor included:

$$\int_{\mathfrak{R}} \mathrm{d}q_x L(\Psi|\theta, q_x, 0)\exp(-2ikq_x \cos\theta \sin\tfrac{1}{2}\alpha')$$

$$= \frac{\psi(\theta - \tfrac{1}{2}\alpha')^*\psi(\theta + \tfrac{1}{2}\alpha')}{|\cos\theta \cos\tfrac{1}{2}\alpha'|}. \quad (35)$$

Through a simple change of variables, Eq. (35) can be written as

$$\psi(\theta)^*\psi(\theta') = \frac{|\cos\theta + \cos\theta'|}{2}$$

$$\times \int_{\Re} dq_x L[\Psi|\tfrac{1}{2}(\theta + \theta'), q_x; 0]$$

$$\times \exp[ikq_x(\sin\theta - \sin\theta')]$$

$$= \frac{|\cos\theta + \cos\theta'|}{2} \int_{\Re} dq_x$$

$$\times M[\Psi|\tfrac{1}{2}(\theta + \theta'), q_x \cos\tfrac{1}{2}(\theta + \theta')]$$

$$\times \exp[ikq_x(\sin\theta - \sin\theta')]. \qquad (36)$$

Now by fixing either θ or θ', this result can be used to extract the wave field to within a global constant phase factor. It also follows from Eq. (18) and Eq. (31) that

$$\int_{\mathcal{S}} d\theta L(\Psi|\theta, q_x; q_z) = \int_{\mathcal{S}} d\theta M(\Psi|\theta, q_x \cos\theta - q_z \sin\theta)$$

$$= |\Psi(\mathbf{q})|^2, \qquad (37)$$

so the intensity of the field at any point can be obtained from the integral of either L or M over all the rays that go through that point. Equivalently, the integral of M over all the rays that travel in a given direction yields the spectrum of the field:

$$\int_{\Re} dl M(\Psi|\theta, l) = |\psi(\theta)|^2. \qquad (38)$$

Notice from Eq. (38) that the integral of the angle-impact marginal over all θ and l yields

$$\int_{\mathcal{S}} d\theta \int_{\Re} dl M(\Psi|\theta, l) = \int_{\mathcal{S}} d\theta \psi(\theta)^*\psi(\theta) = (\Psi, \Psi)_{\mathcal{L}^2(\mathcal{S})}, \qquad (39)$$

where $(\Psi, \Psi)_{\mathcal{L}^2(\mathcal{S})}$ is the norm in the Helmholtz Hilbert space $\mathcal{L}^2(\mathcal{S})$ over the circle.[7] This norm is invariant under translations and rotations.[12] The Helmholtz Hilbert space $\mathcal{L}^2(\mathcal{S})$ over the circle is discussed in Appendix A.

To illustrate the different aspects of the angle-position and angle-impact marginals, we finish this section with some examples. Figure 7 shows (a) the spectral function, (b) the intensity, (c) the angle-position marginal, and (d) the angle-impact marginal for a stationary-monopole field (or Mexican hat function) given by

$$\psi(\theta) = 1, \qquad \text{i.e.,} \quad \Psi(\mathbf{q}) \propto J_0(k|\mathbf{q}|). \qquad (40)$$

Remember that the angle-position and angle-impact marginals are related through the simple mapping given after Eq. (34), and this can be appreciated in Figs. 7(c) and (d). We will therefore show only the angle-impact marginal for the remaining examples. Figure 8 shows the angle-impact marginal for the rectangle beams $\psi(\theta) = \rho(\theta, \pi/16)$ and $\psi(\theta) = \rho(\theta, \pi/4)$. A comparison of Figs. 5(c), 6(c), and 8 shows the similarity between the screen marginal at $q_z = 0$ and the angle-impact marginal, particularly for paraxial wave fields. Figure 9 shows (a) the spectral function, (b) the intensity, and (c) the angle-impact marginal for a stationary-dipole wave-field as defined by

$$\psi(\theta) = \cos\theta, \qquad \text{i.e.,} \quad \Psi(\mathbf{q}) \propto J_1(k|\mathbf{q}|)q_z/|\mathbf{q}|. \qquad (41)$$

Figure 10 shows the corresponding plots for the periodic-Gaussian wave field of waist w, defined by the spectral function

$$\psi(\theta) = \gamma(\theta; w) = \Sigma_m \exp(-m^2 w^2 + im\theta). \qquad (42)$$
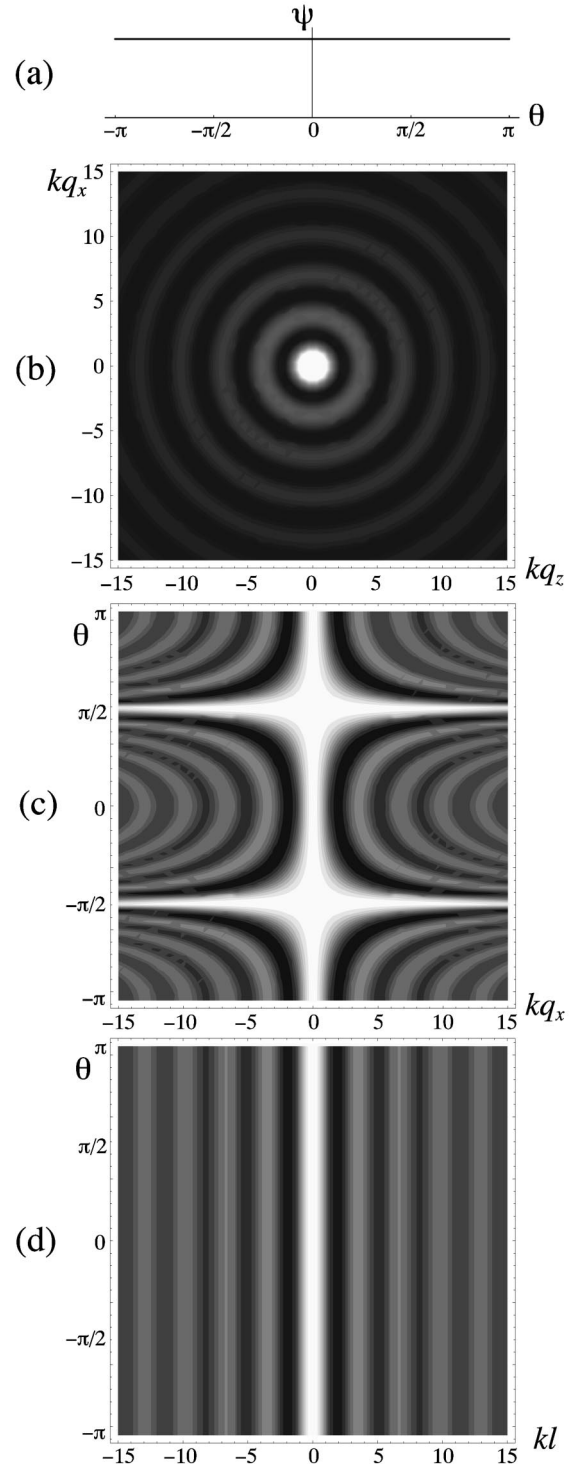
Fig. 7. (a) Spectral function on the circle, (b) intensity, (c) angle-position marginal at $q_z = 0$, and (d) angle-impact marginal, for the Bessel monopole field defined by Eq. (40).
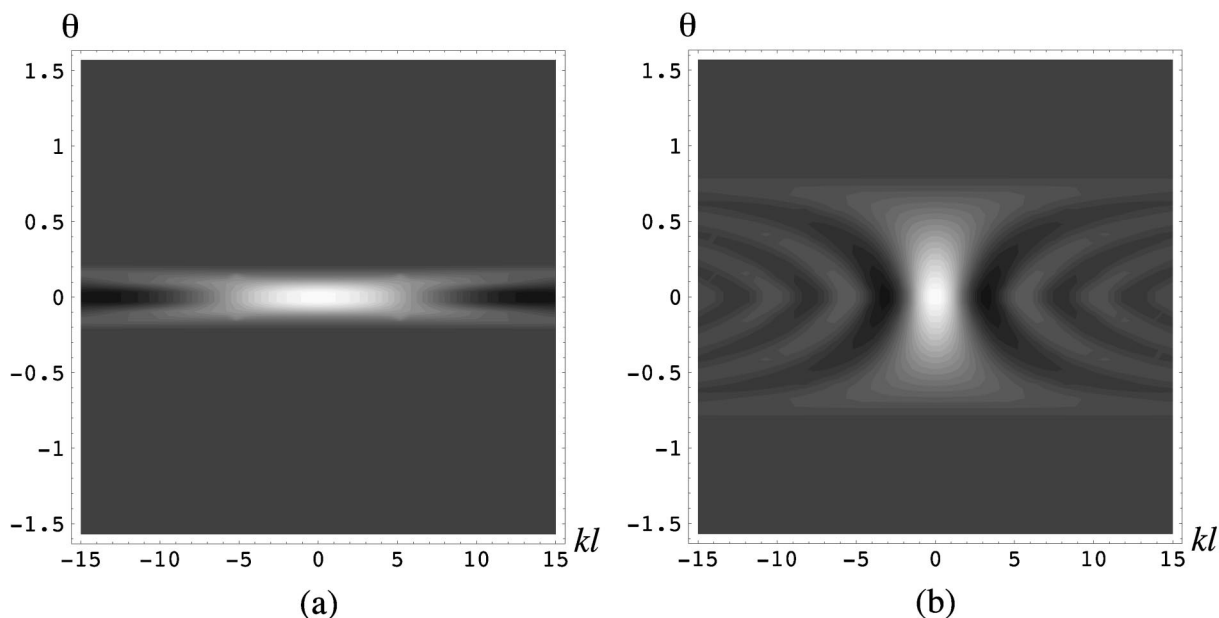
Fig. 8.   Angle-impact marginal for rectangle beams of width $w = \pi/16$ and $w = \pi/4$, as defined by Eq. (20).
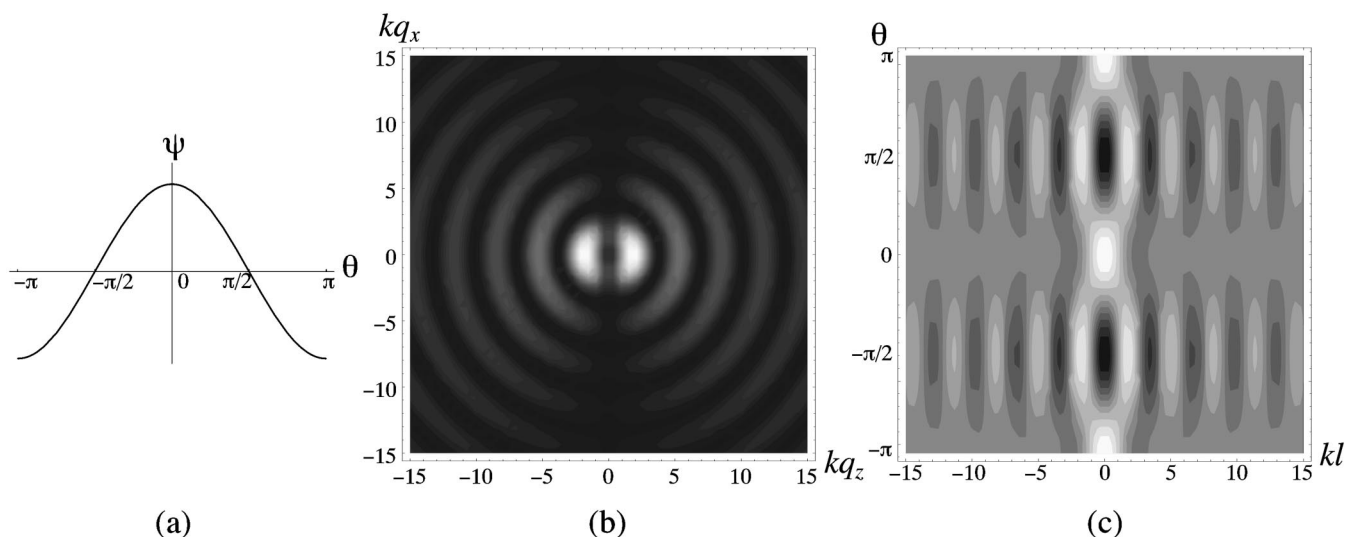
Fig. 9.   (a) Spectral function on the circle, (b) intensity, and (c) angle-impact marginal, for the Bessel dipole field defined by Eq. (41).

Figure 11 shows the superposition of two Gaussian beams displaced in position, namely, $\psi(\theta) = \exp(-ix_0 \sin \theta) \times \gamma(\theta, \omega) + \exp(ix_0 \sin \theta)\gamma(\theta, \omega)$. This type of superposition is analogous to what is known in quantum mechanics as a "Schrödinger-cat state." Note the interference pattern that develops between the two beams. Figure 12 shows a similar "cat state" composed of two such beams displaced in angle, $\psi(\theta) = \gamma(\theta - \theta_0, \omega_0) + \gamma(\theta + \theta_0, \omega_0)$. In this case, two interference patterns develop. The more intense one is centered on the bisectrix of the smaller angle.

7.   CONCLUDING REMARKS

Although the Wigner function of a Helmholtz wave field is not integrable over all its arguments, its zeroth- and first-order moments of momentum are physically meaningful—they give, respectively, the intensity and energy-flux density of the wave field. Negative regions of the Wigner function have been shown to be associated with the phenomenon of a locally backward-pointing flux for a purely forward-propagating wave field. Of course, no measurement process can yield the local value of the flux at a point; only a weighted average over a small region with extent of the order of a wavelength is accessible. One can then expect any measurement to yield only forward values for energy flux. (This is analogous to the well-known measurement process in quantum mechanics through overlap of two Wigner functions, which always yields strictly nonnegative results, even though the Wigner functions generally take negative values.)

A complete and more useful description of a Helmholtz wave field is given by certain marginals of the Wigner function. We have concentrated here on the marginals
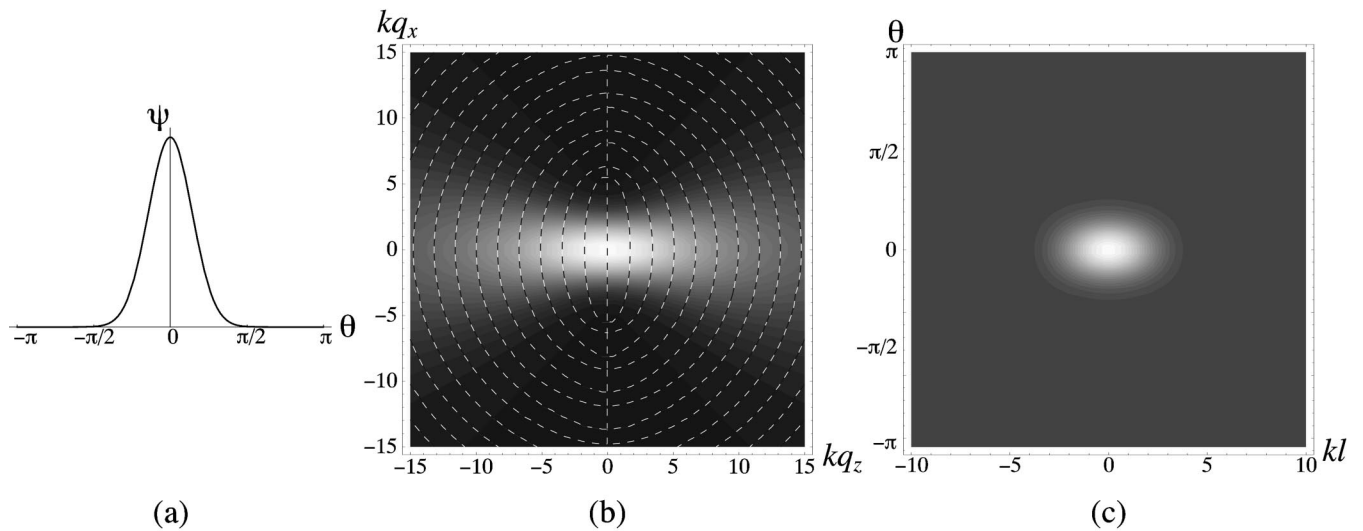
Fig. 10. (a) Spectral function on the circle, (b) intensity and wave fronts of the wave field on the **q** plane, and (c) angle-impact marginal, for the Gaussian wave field defined by Eq. (42) of waist $w^2 = 0.1$.
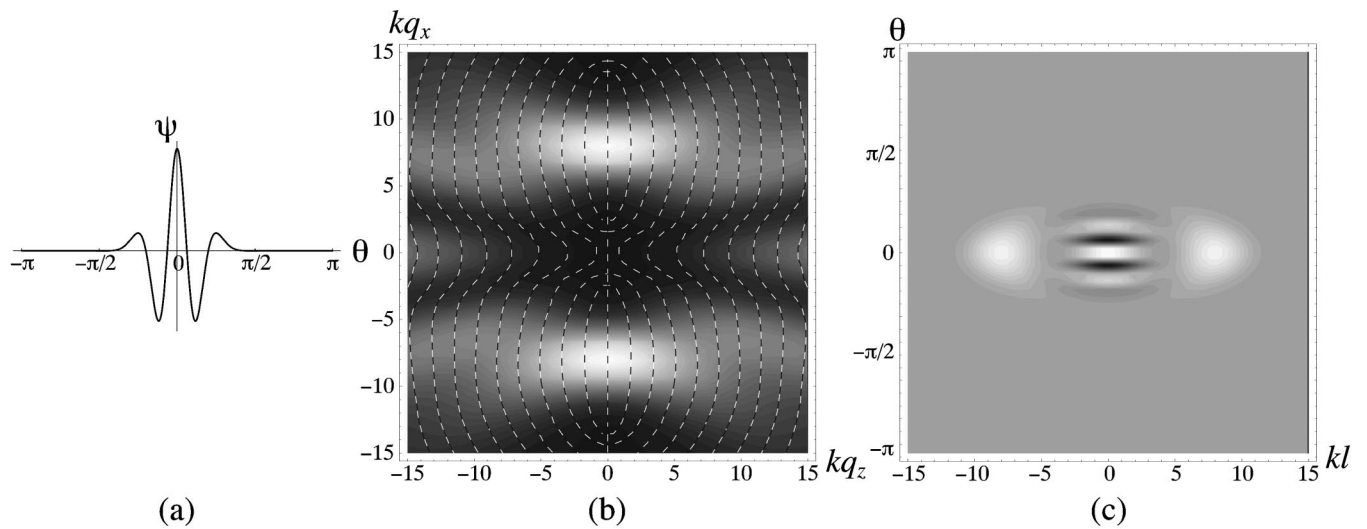
Fig. 11. (a) Spectral function on the circle, (b) intensity and wave fronts of the wave field on the **q** plane, and (c) angle-impact marginal, for the superposition of two Gaussian beams displaced in position along the $q_z = 0$ line.
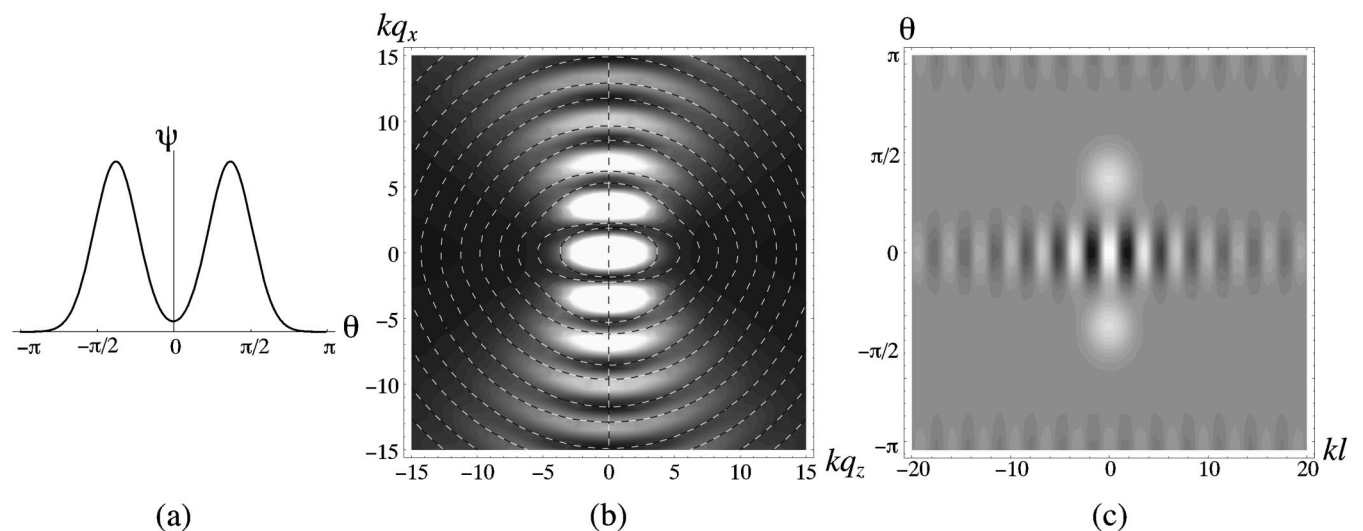
Fig. 12. (a) Spectral function on the circle, (b) intensity and wave fronts of the wave field on the **q** plane, and (c) angle-impact marginal, for the superposition of two Gaussian beams displaced in angle, centered at $\theta = (1/2)\pi$.

that result from projections along either p_z or $|\mathbf{p}|$. The first one, referred to here as the screen marginal, has been used frequently in optics and is a function of three parameters, one of which becomes redundant only when the field propagates paraxially in either the forward or the backward z direction. The second one, the angle-position marginal, is proposed here we believe for the first time and is also a function of three parameters, although one of them is truly redundant. This marginal can therefore be written in terms of a function (the angle-impact marginal) of only two variables. These variables turn out to be the direction and the impact parameter (or angular momentum) of a straight trajectory, so the value of this distribution is manifestly conserved along a ray. Unlike the screen marginal, these new marginals are fully covariant. Further, by integrating the angle-impact marginal over all the rays that go through any given point, it is possible to compute the intensity of the wave field at that point; see Eq. (37). Similarly, integration over the impact parameter yields the modulus of the spectral function as shown in Eq. (38). It follows that the angle-impact marginal extends all the valuable properties of the conventional screen marginal for nonparaxial fields. (It is convenient that in the paraxial limit the angle-impact marginal converges on the conventional screen marginal.) Throughout this work, we have assumed that the wave field is coherent. Nevertheless, the results are also valid for partially coherent fields when ensemble averages are used in the definitions of the different marginals.

Three-dimensional Helmholtz wave fields, where the phase space now has one more pair of Cartesian coordinates, can be treated in a similar manner. Under Fourier transformation, plane waves map to Dirac δ's in momentum that are constrained to lie on a sphere of unit radius, as in Eq. (4). The angle-position marginal is then found by integrating over p the product of p^2 and the Wigner function. Although the derivation is directly analogous to that for the two-dimensional case, it is considerably more complicated owing to the awkwardness of expressing rotations in spherical coordinates. Littlejohn and Winston[4] also proposed an expression for a phase-space distribution function (at a screen) for the three-dimensional case that is conserved along rays. This function, like the angle-position marginal, reduces to the screen marginal in the paraxial case. However, as opposed to the angle-position and angle-impact marginals, this function is tailored to purely forward-propagating fields. As a result, it cannot be covariant under rotations. The angle-impact marginal therefore brings a new intuitive option with extended generality.

APPENDIX A: HILBERT SPACE $\mathcal{L}^2(\mathcal{S})$ OVER THE CIRCLE

As discussed in Section 3, two-dimensional Helmholtz wave fields are not vectors of an $\mathcal{L}^2(\mathfrak{R}^2)$ Hilbert space. Here we give the briefest review of the Helmholtz Hilbert space $\mathcal{L}^2(\mathcal{S})$ over the circle,[7,13] built on the realization of the wave fields $\Psi(\mathbf{q})$ by their spectral functions $\psi(\theta)$, namely,

$$(\Phi, \Psi)_{\mathcal{L}^2(\mathcal{S})} = \int_{\mathcal{S}} \mathrm{d}\theta \phi(\theta)^* \psi(\theta). \tag{A1}$$

By using Helmholtz wave analysis (6) to substitute for $\psi(\theta)$ the values of the field and its normal derivative at the $q_z = 0$ standard screen $\Phi(q_x)$ and $\Psi_z(q_x)$ in Eq. (A1), one obtains a two-fold nonlocal form for the inner product, which we write in convenient 2×2 vector-cum-matrix notation,

$$(\Phi, \Psi)_{\mathcal{L}^2(\mathcal{S})} = \int_{\mathfrak{R}} \mathrm{d}q_x \int_{\mathfrak{R}} \mathrm{d}q_x' \begin{pmatrix} \Phi(q_x) \\ \Phi_z(q_x) \end{pmatrix}^\dagger$$
$$\times \mathbf{M}_k(q_x - q_x') \begin{pmatrix} \Psi(q_x') \\ \Psi_z(q_x') \end{pmatrix}, \tag{A2}$$

$$\mathbf{M}_k(q) = \frac{1}{8\pi} \int_{\mathcal{S}} \mathrm{d}\theta \begin{bmatrix} k\cos^2\theta & -i\cos\theta \\ i\cos\theta & 1/k \end{bmatrix}$$
$$\times \exp(ikq\sin\theta). \tag{A3}$$

This Hilbert space was built in Ref. 12 out of the requirement of full Euclidean invariance and allowing for nonlocal measures; it is the only inner product with this property.

From parity considerations, it is easy to see that the off-diagonal matrix elements integrate to zero, whereas the diagonal ones give the nonlocal weight functions to express inner product (A2) through

$$\mathbf{M}_k(q) = \tfrac{1}{4} \mathrm{diag}[J_1(kq)/q, J_0(kq)/k]. \tag{A4}$$

Now we define a z-reflection operator, I_z such that $I_z \psi(\theta) = \sigma_z(\theta)\psi(\theta)$, where $\sigma_z(\theta)$ was introduced in Eq. (6) as a sign to distinguish between forward and backward wave fields. Its expectation value between the fields in Eq. (A3) is then

$$(\Phi, I_z\Psi)_{\mathcal{L}^2(\mathcal{S})} = \int_{\mathfrak{R}} \mathrm{d}q_x \int_{\mathfrak{R}} \mathrm{d}q_x' \begin{pmatrix} \Phi(q_x) \\ \Phi_z(q_x) \end{pmatrix}^\dagger$$
$$\times \mathbf{I}_k(q_x - q_x') \begin{pmatrix} \Psi(q_x') \\ \Psi_z(q_x') \end{pmatrix}, \tag{A5}$$

where the integral kernel (in 2×2 matrix notation) is Eq. (A3), only with the extra factor of $\sigma_z(\theta)$ inside the integral. Again, simple parity considerations show that now the diagonal matrix elements are zero, while the antidiagonal ones give

$$\mathbf{I}_k(q) = \frac{i}{2k} \frac{1}{\pi} \frac{\sin kq}{q} \begin{bmatrix} 0 & -1 \\ 1 & 0 \end{bmatrix}. \tag{A6}$$

The quantity in parentheses is the reproducing kernel for functions on $\mathfrak{R}$ whose Fourier transform has support on $[-1, 1]$. Therefore Eq. (A6) replaced in Eq. (A5) yields the local integral

$$(\Phi, I_z\Psi)_{\mathcal{L}^2(\mathcal{S})} = \frac{1}{2ik} \int_{\mathfrak{R}} \mathrm{d}q_x [\Phi_z(q_x)^*$$
$$\times \Psi(q_x) - \Phi(q_x)^* \Psi_z(q_x)]. \tag{A7}$$

When $\Phi = \Psi$, this is the flux, defined in Eq. (19), integrated over the x axis. The inner product [Eq. (A1)] is invariant under Euclidean transformations, and the inte-

gration axis can be rotated and translated as fit to accommodate for reflections across the z or any other axis, defining thus a vector flux integral associated with any given line.

The introduction of a proper Hilbert space on the oscillatory solutions of the Helmholtz equation allows for the observability of a system in a given state Ψ by a probe state Φ to be formulated as in quantum mechanics. The expectation value of a quantity that changes sign under reflection can be understood similarly as the flux over the reflection line. It does not give operational meaning to the value of a field at a point, because any probe function must also be a Helmholtz wave field and cannot be narrower than the Mexican-hat function $\sim J_0(kq)$. We observe that the width of the backward-flux regions in Figs. 8 and 9 is smaller than the width of this state.

ACKNOWLEDGMENTS

REFERENCES AND NOTES

1. E. Wigner, "On the quantum correction for thermodynamic equilibrium," Phys. Rev. **40**, 749–759 (1932); H.-W. Lee, "Theory and application of the quantum phase-space distribution functions," Phys. Rep. **259**, 147–211 (1995).
2. A. Walther, "Radiometry and coherence," J. Opt. Soc. Am. **58**, 1256–1259 (1968).
3. A. Walther, "Radiometry and coherence," J. Opt. Soc. Am. **63**, 1622–1623 (1973).
4. R. G. Littlejohn and R. Winston, "Corrections to classical radiometry," J. Opt. Soc. Am. A **10**, 2024–2037 (1993).
5. Yu. A. Kravtsov and Yu. A. Orlov, *Geometrical Optics of Inhomogeneous Media* (Springer-Verlag, Berlin, 1990), p. 23.
6. The existence of an invertible Fourier transform [Eq. (3)] of a (twice-differentiable) Helmholtz wave field $\Psi(\mathbf{q})$ is ensured by the conditions of the Fourier integral theorem only when it is absolutely integrable and of bounded variation. Plane waves are in this sense limit functions for which Fourier analysis can be extended as usual with Dirac δs in the $\mathbf{p}$ plane and on the unit circle [Eq. (4)]. However, evanescent solutions (i.e., of exponential growth in the plane) do not possess a Fourier transform.
7. P. González-Casanova and K. B. Wolf, "Interpolation for solutions of the Helmholtz equation," Num. Meth. Partial Diff. Eqs. **11**, 77–91 (1995).
8. For other references about flux vortices see, for example, M. V. Berry, "Evanescent and real waves in quantum billiards and Gaussian beams," J. Phys. A Nucl. Math. Gen. **27**, L391–L398 (1994).
9. A. Lohmann, "The Wigner function and its optical production," Opt. Commun. **42**, 32–37 (1980).
10. K. B. Wolf and A. L. Rivera, "Holographic information in the Wigner function," Opt. Commun. **144**, 36–42 (1997).
11. M. Bastiaans, "The Wigner distribution function applied to optical signals and systems," Opt. Commun. **25**, 26–30 (1978); "Wigner distribution function and its application to first-order optics," J. Opt. Soc. Am. **69**, 1710–1716 (1979); "The Wigner distribution function and Hamilton's characteristics of a geometric-optical system," Opt. Commun. **30**, 321–326 (1979).
12. S. Steinberg and K. B. Wolf, "Invariant inner products on spaces of solutions of the Klein–Gordon and Helmholtz equations," J. Math. Phys. **22**, 1660–1663 (1981).
13. L. M. Nieto, N. M. Atakishiyev, S. M. Chumakov, and K. B. Wolf, "Wigner distribution function for finite systems," J. Phys. A Nucl. Math. Gen. **31**, 3875–3895 (1998).